

Light hadron spectroscopy in quenched QCD with overlap fermions.*

**Ronald Babich^a, Federico Berruto^b, Nicolas Garron^c, Christian Hoelbling^d,
Joseph Howard^a, Laurent Lellouch^e, Claudio Rebbi^{†a}, and Noam Shoresh^f**

^a*Department of Physics, Boston University, Boston, MA*

^b*Brookhaven National Laboratory, Upton, NY*

^c*DESY, Platanenallee 6, 15738 Zeuthen, Germany*

^d*Department of Physics, Bergische Universität Wuppertal, Germany*

^e*Centre de Physique Théorique[‡] Marseille, France*

^f*Harvard University, Cambridge, MA*

E-mail: rebbi@bu.edu

A simulation of quenched QCD with the overlap Dirac operator has been carried out using 100 Wilson gauge configurations at $\beta = 6$ on an $18^3 \times 64$ lattice and at $\beta = 5.85$ on a $14^3 \times 48$ lattice. Here we present results for meson masses, meson final state “wave functions,” decay constants, and other observables, as well as details on our algorithmic and data analysis techniques. We also summarize results for baryon masses and quark and diquark propagators in the Landau gauge.

*XXIIIrd International Symposium on Lattice Field Theory
25-30 July 2005
Trinity College, Dublin, Ireland*

*This combined contribution includes content from PoS(LAT2005)024.

[†]Speaker.

[‡]UMR 6207 du CNRS et des universités d’Aix-Marseille I, II et du Sud Toulon-Var, affiliée à la FRUMAM.

1. Introduction

The importance of preserving chiral symmetry on the lattice and the advantages of domain-wall [1, 2] and overlap [3, 4, 5] fermions are well recognized, but these advantages come at a heavy computational cost. It is therefore necessary to subject these formulations to the test of simulations on lattices of realistically large size in order to explore the adequacy of available numerical techniques and verify the benefits expected to follow from the preservation of chiral symmetry. In this contribution we present the results of one such investigation with the overlap Dirac operator.

Quenched gauge configurations were generated with the Wilson gauge action at $\beta = 6$ on a lattice of size $18^3 \times 64$, as well as at $\beta = 5.85$ on a $14^3 \times 48$ lattice in order to test scaling. The corresponding values of the lattice spacing are $a^{-1} = 2.12$ GeV and $a^{-1} = 1.61$ GeV, on the basis of the Sommer scale defined by $r_0^2 F(r_0) = 1.65$, $r_0 = 0.5$ fm [6]. The two lattices are therefore of approximately the same physical volume. For 100 configurations at each of the two lattice sizes, overlap quark propagators were calculated for a single point source and all color-spin combinations using a conjugate gradient multimass solver, after gauge-fixing to the Landau gauge. Propagators were calculated for quark masses $am_q = 0.03, 0.04, 0.06, 0.08, 0.1, 0.25, 0.75$ on the $18^3 \times 64$ lattice and $am_q = 0.03, 0.04, 0.053, 0.08, 0.106, 0.132, 0.33, 0.66, 0.99$ on the coarser $14^3 \times 48$ lattice.

Implementation of the overlap operator requires the calculation of $H/\sqrt{H^\dagger H}$ where $H = \gamma_5(D_W - \rho/a)$, and D_W is the Wilson Dirac operator. This was accomplished using a Zolotarev optimal rational function approximation with 12 poles for the first 55 configurations on the $18^3 \times 64$ lattice. A Chebyshev polynomial approximation was used for all remaining configurations after it was found to be about 20 percent more efficient. In both cases, the lowest (12 for 18×64 , 40 for $14^3 \times 48$) eigenvectors of H^2 were first computed with a Ritz algorithm and projected out before inverting the Dirac operator. As convergence criteria we required $|1/\sqrt{H^2} - \sum T_n(H^2)| < 10^{-8}$ and $|D^\dagger D\psi - \chi| < 10^{-7}$. The parameter ρ in the definition of the overlap operator was chosen so as to maximize locality and set to $\rho = 1.4$ at $\beta = 6$ and $\rho = 1.6$ at $\beta = 5.85$ [7, 8]. For further details of the simulation, as well additional results and greater discussion of the results presented herein, see [9].

In the sections that follow, we present results for the meson spectrum, meson final state wave functions, the baryon spectrum, and quark and diquark propagators calculated in the Landau gauge.

2. Light meson observables

2.1 Pseudoscalar spectrum and quenched chiral logarithms

In this and the following three sections, we present results obtained on the finer lattice at $\beta = 6$. A comparison of the two lattices will follow in Section 2.5. We first consider meson correlation functions constructed with point sources and sinks. The general zero-momentum meson correlator is given by

$$G_{AB}(t) = \left\langle \sum_{\vec{x}} \text{Tr} \left[S^{f_2}(0; \vec{x}, t) \Gamma_A \gamma_5 (S^{f_1}(0; \vec{x}, t))^\dagger \gamma_5 \Gamma_B \right] \right\rangle, \quad (2.1)$$

where $S^{f_i}(0; \vec{x}, t)$ is the Euclidean propagator for a quark of flavor f_i , and Γ_A and Γ_B are the appropriate γ -matrix combinations for the states of interest. To extract ground state meson masses,

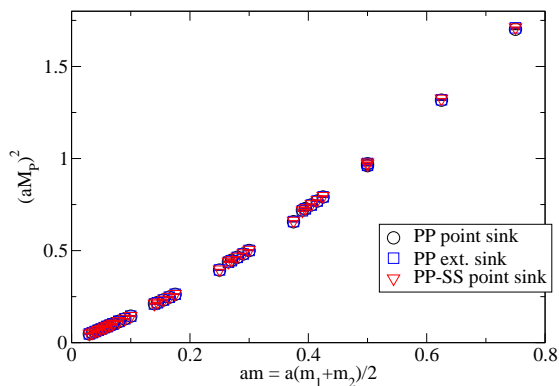


Figure 1: Pseudoscalar meson spectrum for both point and extended sinks.

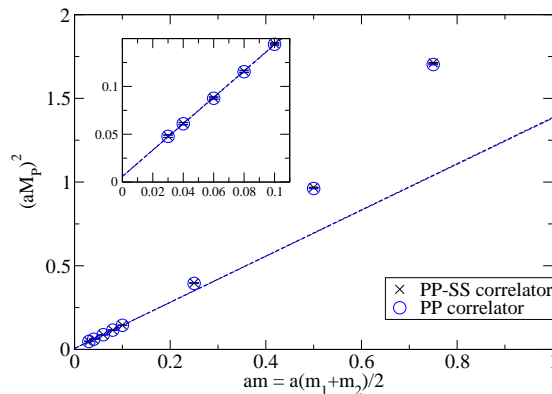


Figure 2: Chiral fit of pseudoscalar meson masses.

correlators were fit to the usual functional form

$$G(t) = \frac{Z}{M} e^{-MT/2} \cosh \left[M \left(\frac{T}{2} - t \right) \right], \quad (2.2)$$

where M is the meson mass, T is the extent of the lattice in time, and we refer to Z as the correlator matrix element. Fits were performed within specified windows $t_{min} \leq t \leq 32a$, which were determined by effective mass estimates and by scanning candidate values of t_{min} to find the smallest value (consistent with the errors) before the clear effect of higher states caused the mass prediction to rise. Errors in the meson masses were estimated with the bootstrap method with 300 samples.

We plot in Fig. 1 our results for the pseudoscalar spectrum for all possible input quark mass combinations. The figure also includes results for correlators with extended sinks, which will be discussed in the next section. In the quenched approximation at finite volume, the correlator $G_{PP}(t)$ receives contributions proportional to $1/m^2$ and $1/m$ from chiral zero modes that are not suppressed by the fermionic determinant. These may be eliminated by considering the difference of pseudoscalar and scalar meson correlators $G_{PP-SS}(t) = G_{PP}(t) - G_{SS}(t)$, since the quenching artifacts cancel by chirality in the difference [10]. On our large lattice no significant differences between the results obtained with PP and $PP - SS$ correlators were observed. Except where noted, we therefore make use of PP correlators in the remainder of this section.

Neglecting for the moment chiral logarithms, we fit the pseudoscalar correlators to the linear form

$$(aM_P)^2 = \mathcal{A} + \mathcal{B}(am), \quad (2.3)$$

for quark masses $am \leq 0.1$. This yields $\mathcal{A} = 0.0058(15)$, $\mathcal{B} = 1.376(15)$ for the PP correlator and $\mathcal{A} = 0.0059(16)$, $\mathcal{B} = 1.380(17)$ for the $PP - SS$ correlator. The nonzero value of the intercept \mathcal{A} is statistically significant, and the $PP - SS$ result confirms that it is not attributable to zero modes. The deviation from linear behavior must therefore be due either to finite volume effects or to chiral logarithms. Regarding finite volume effects, we can note that the Compton wavelength of our lightest pseudoscalar, $M_P^{-1} \approx 4.5a$, is much smaller than the lattice size $L = 18a$ ($M_P L = 4$).

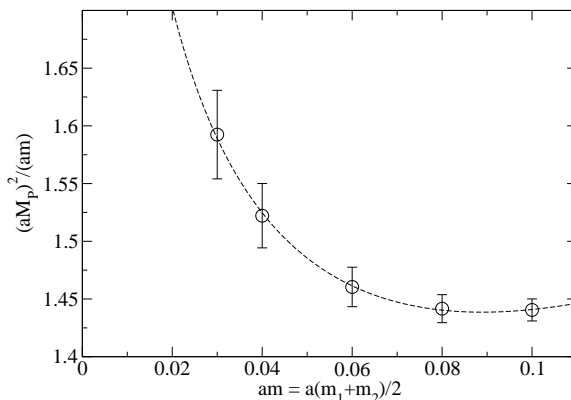


Figure 3: Evidence for quenched chiral logs.

We proceed to test the supposition of quenched chiral logs, and fit the degenerate quark mass results for the pseudoscalar masses to the expression [11]

$$(aM_P)^2 = A(am)^{1/(1+\delta)} + B(am)^2, \quad (2.4)$$

where the leading quenched logarithms have been resummed into a power behavior, and the term proportional to B parameterizes possible higher-order corrections in the mass expansion. The resulting fit is shown in Fig. 3, plotted in terms of the ratio $(aM_P)^2/am$, which exhibits a sharp rise at small m . This yields $A = 0.680(68)$, $B = 2.98(31)$, $\delta = 0.29(5)$, consistent with values of δ presented elsewhere in the literature.

2.2 Extended sinks and vector meson spectrum

For some correlation functions, such as the vector VV correlators, signals may be greatly improved by the use of extended sources and sinks. As a practical constraint, we were forced to generate quark propagators for point sources, as these were required for the study of nonperturbative renormalization and the evaluation of selected matrix elements. We were free to take advantage of extended sinks, however, which were constructed for PP and VV correlators as follows.

In the Landau gauge, we define a correlation function dependent on the separation r between the quark and antiquark at the sink [12] by

$$G(r, t) = \sum_{\vec{x}, \vec{y}} \{ \text{Tr} [S^{f_2}(0; \vec{x}, t) \Gamma_A \gamma_5 (S^{f_1}(0; \vec{y}, t))^\dagger \gamma_5 \Gamma_B] \delta(|\vec{x} - \vec{y}| - r) \}. \quad (2.5)$$

In calculating this function, a fast Fourier transform was used to reduce the double summation over spatial lattice sites to a single sum, decreasing the computational time by almost three orders of magnitude [13]. Figure 4 shows the mean value of the $G(r, t)$ correlators for pseudoscalar mesons with quark mass $am = 0.03$, each normalized to unity at $r = 0$. A clear ground state “wave function” is apparent after about $t/a = 8$. For both the PP and VV correlators, we used the corresponding functions $\varphi(r) \equiv G(r, 8a)$ to define extended sink correlators

$$G_{\text{ext}}(t) = \sum_r \varphi(r) G(r, t), \quad (2.6)$$

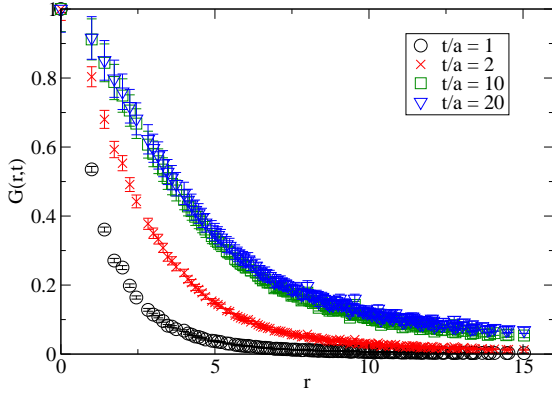


Figure 4: PP extended sink correlators $G(r,t)$ at various t for $am_1 = am_2 = 0.03$.

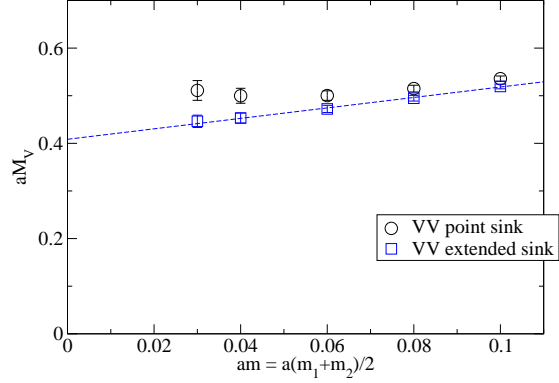


Figure 5: Vector meson spectrum for $am \leq 0.1$.

from which we then extracted the meson masses.

The use of extended sinks was most valuable in the calculation of the vector meson spectrum. The point sink and extended sink vector meson spectra are compared in Fig. 5 for small quark masses $am \leq 0.1$. A linear fit of the extended sink data gives $aM_V = 0.409(15) + 1.10(13)(am)$. We note that the chiral limit value of $0.409(15)$ is larger than the value 0.366 obtained using the lattice spacing as determined by the Sommer scale and the experimental ρ mass, giving an indication of the systematic error induced by the quenched approximation.

2.3 Axial Ward identity and Z_A

Exact chiral symmetry implies a conserved axial current, and the associated axial Ward identity (AWI) predicts a constant value for the ratio

$$\rho(t) = \frac{G_{\nabla_0 A_0 P}(t)}{G_{PP}(t)}. \quad (2.7)$$

The conserved axial current is a local, but not ultralocal, operator. The ultralocal axial current

$$A_0 = \bar{\psi}_1(x) \gamma_0 \gamma_5 \left[\left(1 - \frac{a}{2\rho} D\right) \psi_2 \right] (x) \quad (2.8)$$

differs from the exactly conserved axial current by a finite renormalization factor Z_A and possible corrections $\mathcal{O}(a^2)$. We calculated the correlator in Eq. (2.7) with the current of Eq. (2.8) and using the lattice central difference for ∇_0 , corrected so as to take into account the sinh behavior of the correlator. Figure 6 shows the observation of plateaus for all available quark masses in the range $8 \leq t/a \leq 56$.

The fit shown in Fig. 7 to

$$a\rho = \mathcal{A} + 2(am)/Z_A + \mathcal{C}(am)^2 \quad (2.9)$$

gives $\mathcal{A} = 0.00002(10)$, $Z_A = 1.5555(47)$, $\mathcal{C} = 0.273(32)$. The fact that \mathcal{A} is consistent with zero is an excellent indication of the good chiral behavior of the overlap formulation (compared to the residual mass found in domain-wall fermion calculations). We also note that \mathcal{C} is rather small, possibly indicating that discretization errors might be smaller than expected on the basis of purely dimensional arguments.

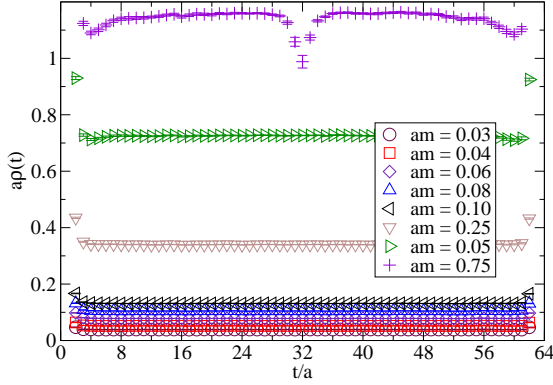


Figure 6: AWI ratio as a function of time for all degenerate quark mass combinations.

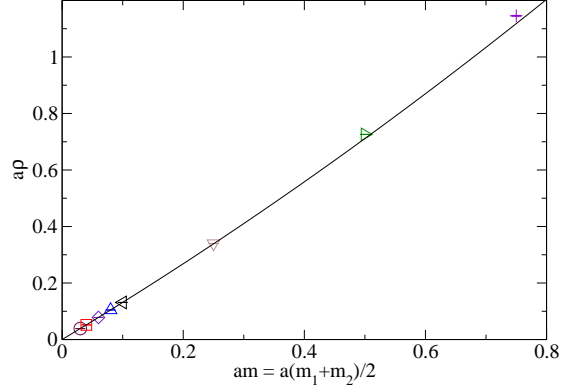


Figure 7: Axial Ward identity fit.

2.4 Quark masses and chiral condensate

Using our data for the pseudoscalar spectrum together with the experimental value for the kaon mass rescaled by the lattice spacing as determined from the Sommer scale, we find $a(m_s + \hat{m}) = 0.0709(17)$ for the sum of the strange and light bare quark masses. A given bare quark mass $m(a)$ is related to the renormalized quark mass $\bar{m}(\mu)$ by

$$\bar{m}(\mu) = \lim_{a \rightarrow 0} Z_m(a\mu) m(a) . \quad (2.10)$$

The mass renormalization constant Z_m is in turn related to the renormalization constant Z_S for the non-singlet scalar density by $Z_m(a\mu) = 1/Z_S(a\mu)$. We calculated Z_S in the RI-MOM scheme starting from the identity

$$Z_S^{\text{RI}}(a\mu) = \lim_{m \rightarrow 0} Z_A \frac{\Gamma_A(p, m)}{\Gamma_S(p, m)} \Big|_{p^2 = \mu^2} , \quad (2.11)$$

where $\Gamma_A(p, m)$ and $\Gamma_S(p, m)$ are suitably defined quark two-point functions for the axial current and the scalar density in the Landau gauge, and Z_A is the renormalization constant for the axial current calculated in the previous section. Details of the procedure will be presented in a forthcoming publication. From it we find $Z_S^{\text{RI}}(2\text{GeV}) = 1.195(9)(27)$, where the first error is statistical and the second systematic. With this result, one can use the three-loop perturbative calculation of the ratio $Z_S^{\overline{\text{MS}}}/Z_S^{\text{RI}}$ [14] to calculate $Z_S^{\overline{\text{MS}}}(2\text{GeV}) = 1.399(10)(32)$. Using this value, we find $(m_s + \hat{m})^{\overline{\text{MS}}}(2\text{GeV}) = 107(4)(2)$ MeV for the sum of strange and light quark masses. Finally, using the value $m_s/\hat{m} = 24.4(1.5)$ from chiral perturbation theory [15], we obtain $m_s^{\overline{\text{MS}}}(2\text{GeV}) = 103(4)(2)$ MeV for the strange quark mass.

We have also calculated the chiral condensate by performing a fit to the mass dependence of the quantity

$$-a^3 \tilde{\chi}(m) = am \sum_x (\langle P(x) P^c(0) \rangle - \langle S(x) S^c(0) \rangle) , \quad (2.12)$$

where the superscript c denotes interchange of the two quark flavors. A quadratic fit gives $-a^3 \tilde{\chi} = 0.00131(8)$ for the value at zero quark mass, yielding $\langle \bar{\psi} \psi \rangle^{\overline{\text{MS}}}(2\text{GeV}) = -0.0175(11)(6) \text{GeV}^3 = -[260(6)(8) \text{MeV}]^3$.

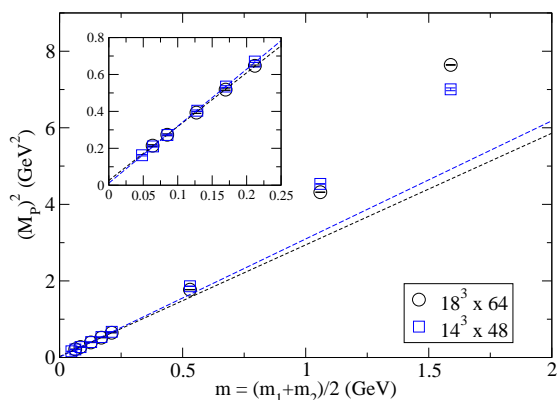
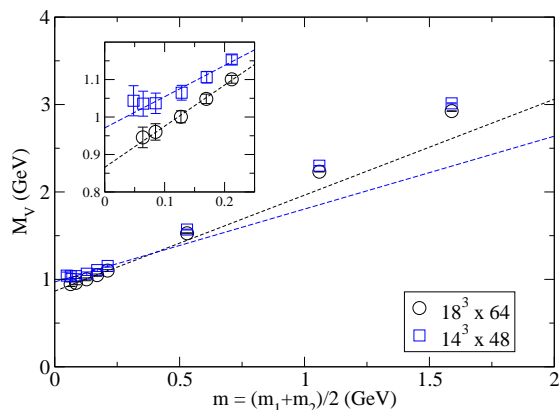
Figure 8: Pseudoscalar PP spectrum comparison.

Figure 9: Vector (extended sink) spectrum comparison.

Quantity	$\beta = 6$	$\beta = 5.85$
Z_A	1.5555(47)	1.4432(50)
δ (degenerate)	0.29(5)	0.17(4)
a^{-1} (Sommer) [6]	2.12 GeV	1.61 GeV
a^{-1} (physical planes)	2.19(6) GeV	1.44(4) GeV
a^{-1} (M_ρ)	1.90(4) GeV	1.28(6) GeV
f_K/f_π	1.13(4)	1.09(4)
f_{K^*}/f_ρ	1.03(6)	1.03(10)
M_{K^*}/M_ρ	1.09(5)	1.08(6)
$Z_S^{\overline{\text{MS}}}(2\text{ GeV})$	1.399(10)(32)	1.290(14)(82)
$(m_s + \hat{m})^{\overline{\text{MS}}}(2\text{ GeV})$	107(4)(2) MeV	117(2)(8) MeV
$m_s^{\overline{\text{MS}}}(2\text{ GeV})$	103(4)(2) MeV	112(2)(8) MeV
$\langle \bar{\psi}\psi \rangle^{\overline{\text{MS}}}(2\text{ GeV})$	$-[260(6)(8)\text{ MeV}]^3$	$-[288(5)(24)\text{ MeV}]^3$

Table 1: Comparison of data for the two lattices.

2.5 Meson scaling

In Figs. 8 and 9, we compare our results for the pseudoscalar and vector spectra on the two lattices, using the lattice spacing determined from the Sommer scale to express masses in physical units. We neglect logarithmic effects in the lattice spacing and plot the mass spectra as a function of bare quark mass. It is interesting to observe that our results for the mass spectra on the two different lattices are very similar, a conclusion that would remain qualitatively unchanged in considering renormalized quark masses. Our results suggest that scaling violations for these quantities may be quite small.

Complete results for the coarser lattice may be found in [9], and we provide a direct comparison of selected quantities in Table 1.

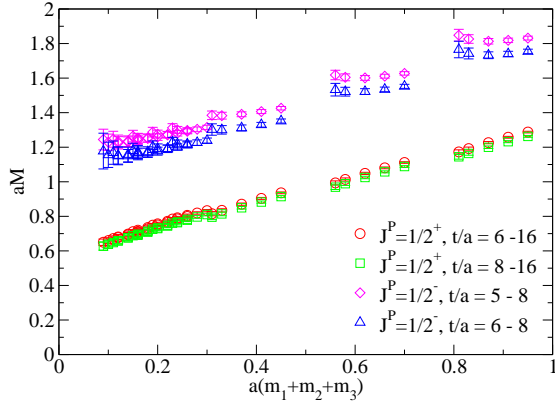


Figure 10: Λ -like octet masses at $\beta = 6$ for two fitting windows and quark masses $m_1 = m_2$ degenerate.

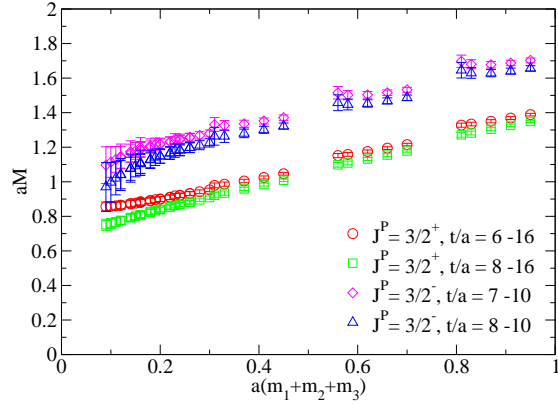


Figure 11: Decuplet masses at $\beta = 6$ for two fitting windows and quark masses $m_1 = m_2$ degenerate.

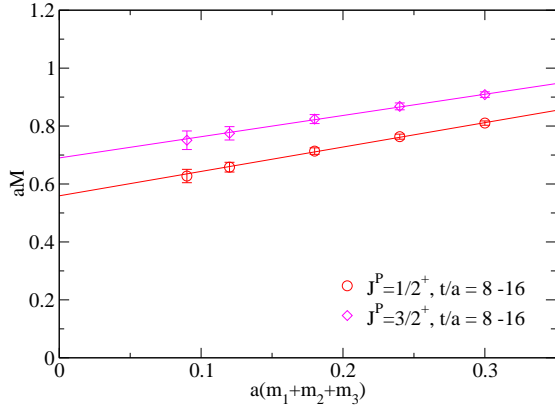


Figure 12: Chiral fit of baryon masses at $\beta = 6$ with three light degenerate quarks.

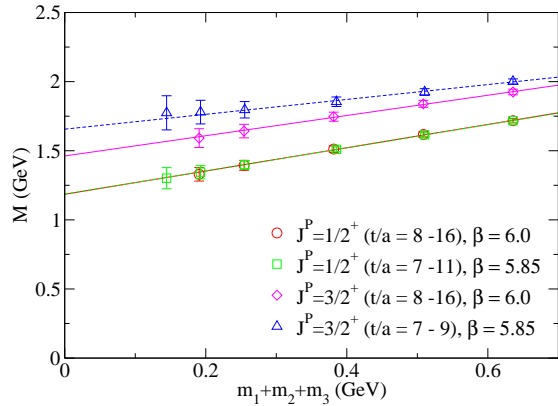


Figure 13: Comparison of baryon masses with light degenerate quarks at two values of β .

3. Baryon spectra

Baryon correlation functions were constructed with point sources and sinks using standard interpolating operators. Uncorrelated single-mass fits were performed within fitting windows chosen on the basis of effective mass plots, and errors were estimated by bootstrap. For the results that follow, baryon masses were calculated with two degenerate quarks having each of the five lightest available masses (six on the $14^3 \times 48$ lattice) and for all available masses of the third quark.

The positive and negative-parity octet masses are plotted in Fig. 10 as a function of total quark mass. Measurements for two values of t_{min} are shown in order to give some indication of the dependence on fitting window. Decuplet spectra are plotted in Fig. 11.

In Fig. 12, we plot the masses of the positive-parity states for light degenerate quark masses $am_q = 0.03, 0.04, 0.06, 0.08, 0.1$. A linear extrapolation to the chiral limit gives $aM_8 = 0.559(24)$ and $aM_{10} = 0.690(32)$. In this limit, we find $M_8/M_\rho = 1.367(77)$ and $M_{10}/M_8 = 1.234(78)$.

Finally, we plot in Fig. 13 the $J^P = \frac{1}{2}^+$ and $J^P = \frac{3}{2}^+$ states for light degenerate quarks on both lattices where bare masses have been rescaled by the corresponding values of a^{-1} set by the

Sommer scale. At $\beta = 5.85$, we find $aM_8 = 0.739(28)$ and $aM_{10} = 1.032(55)$ in the chiral limit, yielding $M_8/M_\rho = 1.222(61)$ and $M_{10}/M_8 = 1.395(91)$. The octet spectrum exhibits good scaling while the decuplet shows some indication of scaling violation. We note, however, that the decuplet masses suffer from greater uncertainty in the choice of fitting window (estimated to be on the same order as the statistical error), and so the apparent lack of scaling has limited significance.

4. Diquark correlations

The possible existence of exotic states such as the Θ^+ pentaquark has given a renewed relevance to diquark models [16]. A study of correlations among quarks in baryons is currently in progress which might provide additional evidence for such models.

The fact that our propagators were calculated in the Landau gauge allows us also to measure quark-quark correlations directly and to fit their decay in Euclidean time in terms of an effective “diquark mass” [17]. Of course, such a mass parameter can only be defined in a fixed gauge and is not the mass of a physical state. Nevertheless, it can give an indication of the relative strength of quark bindings within diquark states. We consider correlation functions for the diquark operators

$$\mathcal{O}_c^{s_1 s_2}(x) = \varepsilon_{cc_1 c_2} \psi_{c_1}^{s_1}(x) \psi_{c_2}^{s_2}(x) \quad (4.1)$$

and

$$\mathcal{O}_{c_1 c_2}^{s_1 s_2}(x) = \frac{1}{\sqrt{2}} (\psi_{c_1}^{s_1}(x) \psi_{c_2}^{s_2}(x) + \psi_{c_2}^{s_1}(x) \psi_{c_1}^{s_2}(x)), \quad (4.2)$$

which are a $\bar{\mathbf{3}}$ and $\mathbf{6}$ of color, respectively. Using these operators, we form four types of diquark states: (i) color $\bar{\mathbf{3}}$, spin-0, flavor $\bar{\mathbf{3}}$, (ii) color $\bar{\mathbf{3}}$, spin-1, flavor $\mathbf{6}$, (iii) color $\mathbf{6}$, spin-0, flavor $\mathbf{6}$, and (iv) color $\mathbf{6}$, spin-1, flavor $\bar{\mathbf{3}}$.

We work in a basis where γ_4 is diagonal, and so to extract the mass of a positive-parity state, correlators involving upper components (Dirac indices 1, 2) are combined with time-reversed lower-component correlators. Negative-parity states are constructed with one upper and one lower component (e.g. 1, 3). Plotted in Fig. 14 are positive-parity diquark correlation functions for the $\bar{\mathbf{3}}$ state with $am_1 = 0.03$ and $am_2 = 0.03$, the lightest available quark mass combination. For comparison we also extract constituent quark masses by performing fits to the quark propagators. Plotted in Fig. 15 is an example for $am_q = 0.03$, giving the constituent quark mass $aM = 0.229(5)$.

In Figs. 16 and 17 we plot the positive and negative-parity diquark spectra, as determined from fits between $t_{min} = 5a$ and $t_{max} = 15a$. Also included are plots of twice the constituent quark mass and extrapolations to the chiral limit for these and the lowest-lying diquark states. It is interesting to observe that in the first plot, the $\bar{\mathbf{3}}$ spin-0 diquark extrapolation is below twice the quark mass extrapolation and that the $\bar{\mathbf{3}}$ spin-0 diquark state is significantly more strongly bound than the $\bar{\mathbf{3}}$ spin-1 diquark. These results are consistent with the predictions of diquark models [16, 18]. We again emphasize, however, that a much more detailed analysis must be done, particularly of diquarks within baryons, before rigorous conclusions may be reached.

5. Conclusions

In this contribution, we have presented results from quenched lattice QCD simulations using the overlap Dirac operator for meson and baryon observables, quark masses, meson final-state

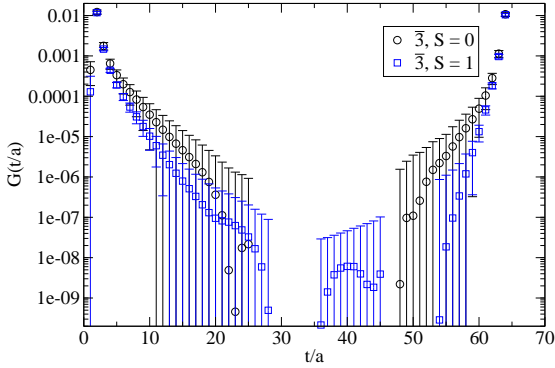


Figure 14: Positive-parity $\bar{3}$ diquark correlators for $am_1 = am_2 = 0.03$ at $\beta = 6$.

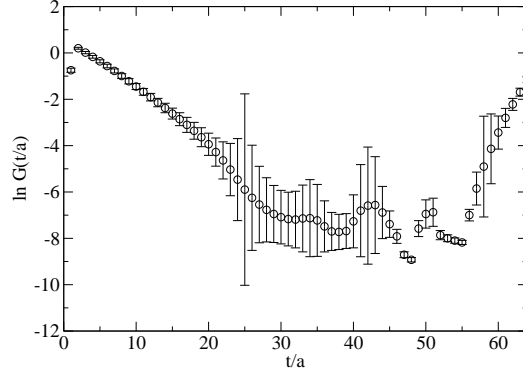


Figure 15: Quark propagator for input quark mass $am = 0.03$ at $\beta = 6$.

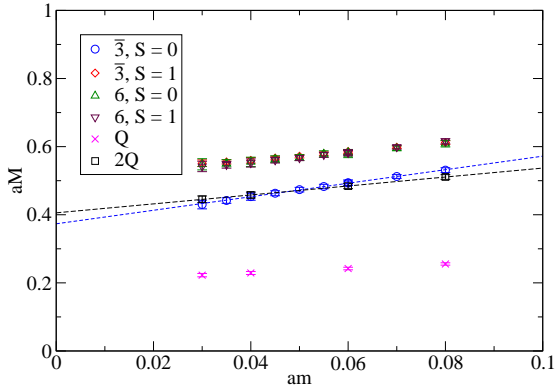


Figure 16: Positive-parity diquark spectra at $\beta = 6$.

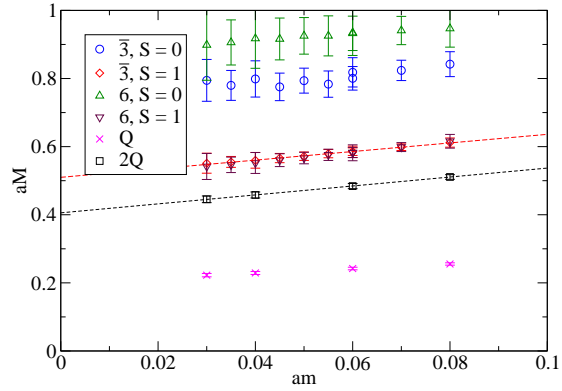


Figure 17: Negative-parity diquark spectra at $\beta = 6$.

wave functions, and diquark correlations. One important result of this work is the demonstration that techniques are mature for calculating propagators with the overlap Dirac operator on large lattices, up to a chosen numerical precision, even with “rough” gauge backgrounds. Improved algorithms or smoothing techniques both may help to make the calculation less computationally demanding [19].

Our investigation also validates the good chiral properties of the overlap operator and demonstrates good scaling properties between $\beta = 5.85$ and $\beta = 6$, indicating that the $\beta = 6$ results may already be close to the continuum limit. In comparisons to experiment, our results suffer from the shortcomings of the quenched approximation. Nevertheless, from this investigation and others it is clear that it should be possible to use the overlap operator in dynamical fermion simulations, at the very least with a mixed action formulation. Work in this direction is beginning.

Acknowledgments

This work was supported in part by US DOE grants DE-FG02-91ER40676 and DE-AC02-98CH10866, EU HPP contract HPRN-CT-2002-00311 (EURIDICE), and grant HPMF-CT-2001-01468. We thank Boston University and NCSA for use of their supercomputer facilities.

References

- [1] D. B. Kaplan, “A Method for simulating chiral fermions on the lattice,” *Phys. Lett.* **B288** (1992) 342–347, hep-lat/9206013.
- [2] Y. Shamir, “Chiral fermions from lattice boundaries,” *Nucl. Phys.* **B406** (1993) 90–106, hep-lat/9303005.
- [3] R. Narayanan and H. Neuberger, “A Construction of lattice chiral gauge theories,” *Nucl. Phys.* **B443** (1995) 305–385, hep-th/9411108.
- [4] R. Narayanan and H. Neuberger, “Chiral determinant as an overlap of two vacua,” *Nucl. Phys.* **B412** (1994) 574–606, hep-lat/9307006.
- [5] H. Neuberger, “Exactly massless quarks on the lattice,” *Phys. Lett.* **B417** (1998) 141–144, hep-lat/9707022.
- [6] ALPHA Collaboration, M. Guagnelli, R. Sommer, and H. Wittig, “Precision computation of a low-energy reference scale in quenched lattice QCD,” *Nucl. Phys.* **B535** (1998) 389–402, hep-lat/9806005.
- [7] P. Hernández, K. Jansen, and M. Luscher, “Locality properties of Neuberger’s lattice Dirac operator,” *Nucl. Phys.* **B552** (1999) 363–378, hep-lat/9808010.
- [8] P. Hernández, K. Jansen, and L. Lellouch, “Finite-size scaling of the quark condensate in quenched lattice QCD,” *Phys. Lett.* **B469** (1999) 198–204, hep-lat/9907022.
- [9] R. Babich *et al.*, “Light hadron and diquark spectroscopy in quenched QCD with overlap quarks on a large lattice,” hep-lat/0509027.
- [10] T. Blum *et al.*, “Quenched lattice QCD with domain wall fermions and the chiral limit,” *Phys. Rev.* **D69** (2004) 074502, hep-lat/0007038.
- [11] S. R. Sharpe, “Quenched chiral logarithms,” *Phys. Rev.* **D46** (1992) 3146–3168, hep-lat/9205020.
- [12] S. A. Gottlieb, “Portrait of a proton,” Presented at Conf. ‘Advances in Lattice Gauge Theory’, Tallahassee, FL, Apr 10-13, 1985.
- [13] S. Hauswirth, “Light hadron spectroscopy in quenched lattice QCD with chiral fixed-point fermions,” hep-lat/0204015.
- [14] K. G. Chetyrkin and A. Retey, “Renormalization and running of quark mass and field in the regularization invariant and \overline{MS} -bar schemes at three and four loops,” *Nucl. Phys.* **B583** (2000) 3–34, hep-ph/9910332.
- [15] H. Leutwyler, “The ratios of the light quark masses,” *Phys. Lett.* **B378** (1996) 313–318, hep-ph/9602366.
- [16] R. L. Jaffe and F. Wilczek, “Diquarks and exotic spectroscopy,” *Phys. Rev. Lett.* **91** (2003) 232003, hep-ph/0307341.
- [17] M. Hess, F. Karsch, E. Laermann, and I. Wetzorke, “Diquark masses from lattice QCD,” *Phys. Rev.* **D58** (1998) 111502, hep-lat/9804023.
- [18] M. Anselmino, E. Predazzi, S. Ekelin, S. Fredriksson, and D. B. Lichtenberg, “Diquarks,” *Rev. Mod. Phys.* **65** (1993) 1199–1234.
- [19] S. Durr, C. Hoelbling, and U. Wenger, “Filtered overlap: Speedup, locality, kernel non-normality and $Z_A \simeq 1$,” hep-lat/0506027.